

**Figure 5-7b: Axial Stresses for the Steady State Condition for the 23.5° Penetration for the Small Diameter Heater Sleeve**

### 5.2.6 EFFECT OF SUPPORT SKIRT ON OUTERMOST HEATER SLEEVE STRESSES

The pressurizer is supported by a cylindrical skirt as shown in Figure 5-8. The base flange of the support skirt is bolted to the floor. At the top of the support skirt is a forging, the knuckle, which forms the connection between the skirt and the pressurizer lower head. The knuckle provides a significant local increase in the stiffness of the lower head. The knuckle produces non uniform radial displacements of the lower head for pressure loads as it acts as a radial constraint for the head.

The effect of the skirt on the stress in the heater sleeve was investigated by performing two different analyses. The first one included the skirt as shown in Figure 5-8. The second analysis was performed using the same model but by ignoring the skirt effects. In this analysis, the material properties for the knuckle and the skirt were assumed to have a stiffness of only 1/1000 their actual stiffness. For both

cases a pressure load of 1000 psi was applied to the inside surface of the head. The operating pressure is 2250 psi, but the comparison of the two cases is not impacted as both were completed with the same pressure. Blow off loads were applied to the end of the surge nozzle, the outside end of the heater sleeve and to the cylindrical end of the pressurizer. Pressure was applied to the inside of the heater sleeve and to the outside surfaces of the sleeve that is inside the pressurizer.

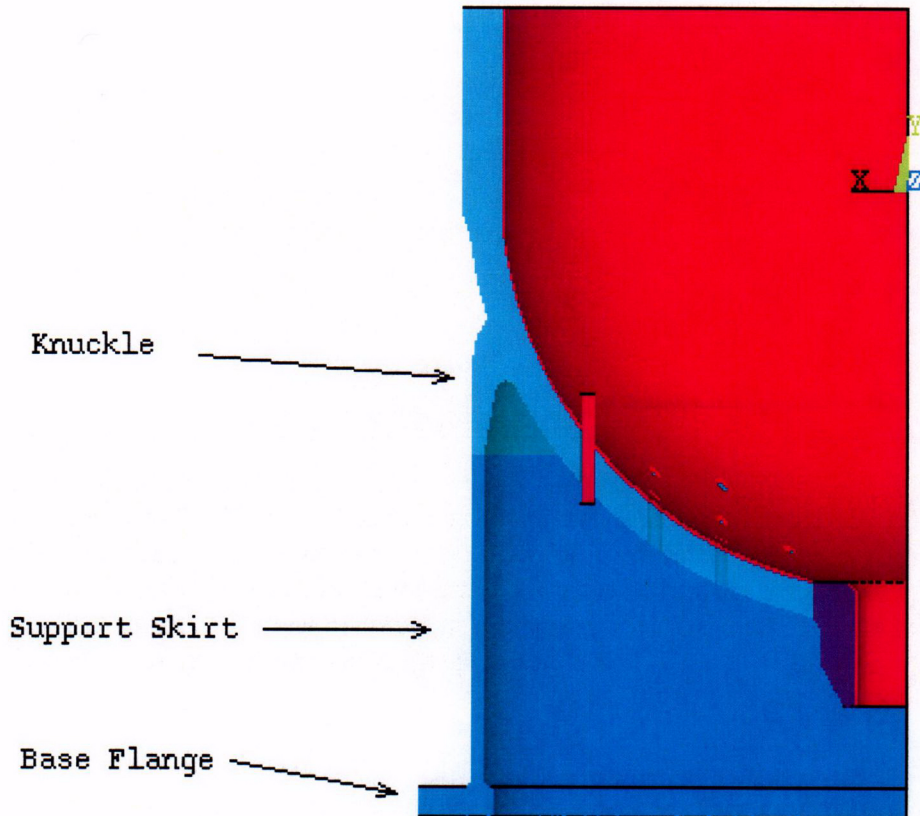


**Figure 5-8: Pressurizer Model with Support Skirt and Outermost Heater Sleeve**

The analysis of the bottom head and skirt structure show that, for the normal operating pressure loadings, the stress levels in the heater sleeves in the region generally remain the same when the presence of the skirt is considered. The stresses do not increase significantly at the outermost heater sleeves when the support skirt is modeled in the analyses.

### 5.2.7 STRESS ANALYSIS RESULTS – MID-PLANE LOCATION

In Alloy 600 nozzle type applications, stress corrosion cracks observed in the field have been at uphill or downhill locations ( $0^\circ$  or  $180^\circ$  locations). Stress analyses indicate that the highest tensile hoop stresses are at these locations rather than mid-way around the circumference of the penetrations where stresses tend to be compressive. For completeness, stresses were also evaluated at the mid-plane or  $90^\circ$  locations in addition to the uphill and downhill locations as described in Sections 5.2.3 through 5.2.5. Hoop and axial stresses at the mid-plane location are shown in Figures 5-9a and b for the small diameter heater sleeve at the outermost ( $59.7^\circ$ ) location. Figures 5-10a and b show the hoop and axial stresses for the large diameter sleeves at the  $35.5^\circ$  location. These locations were selected to show the stresses at mid-plane locations because these are the governing locations for small and large diameter sleeves.

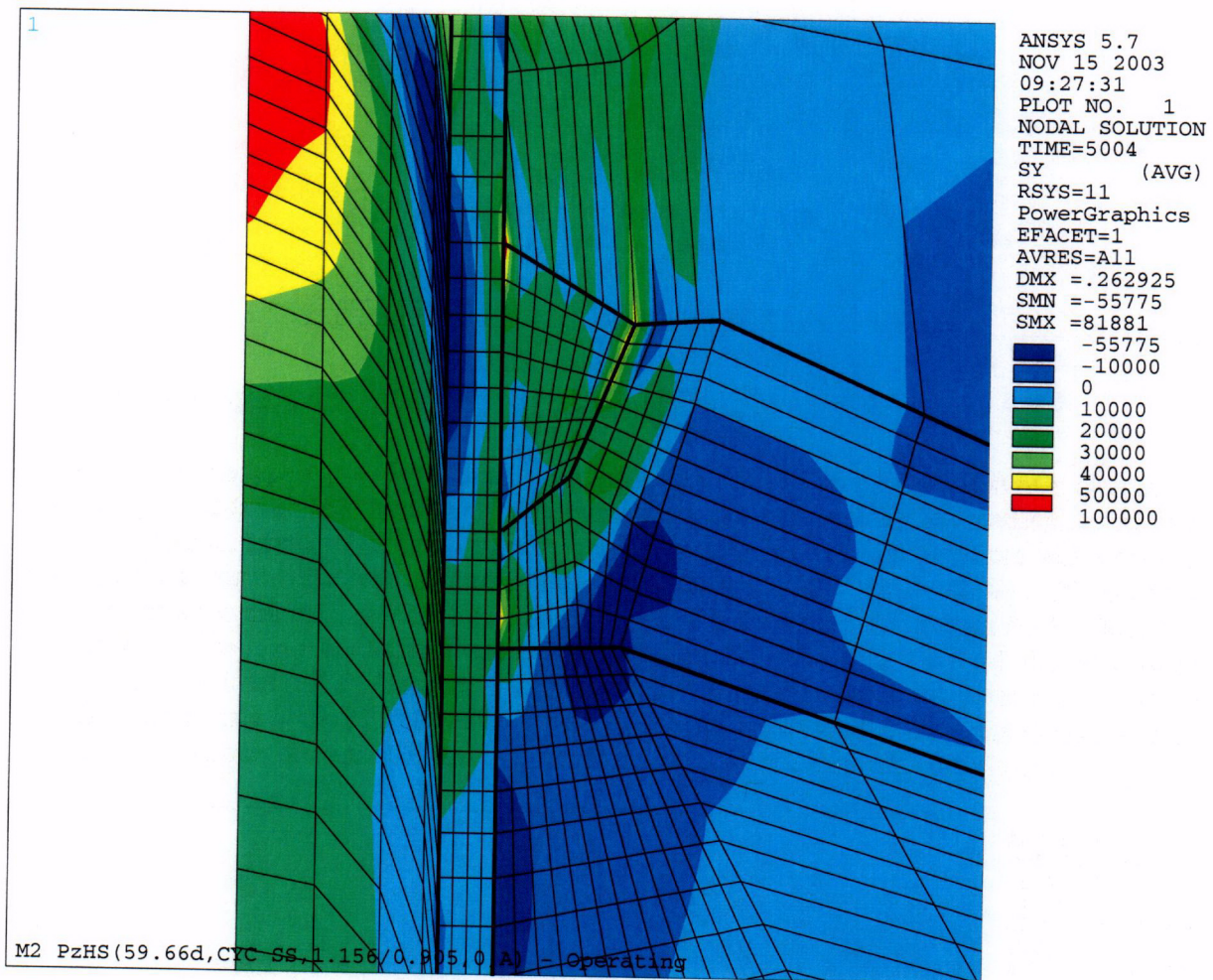


**Figure 5-9a: Mid-plane Hoop Stresses for the Steady State Condition for the  $59.7^\circ$  Penetration for the Small Diameter Heater Sleeve**

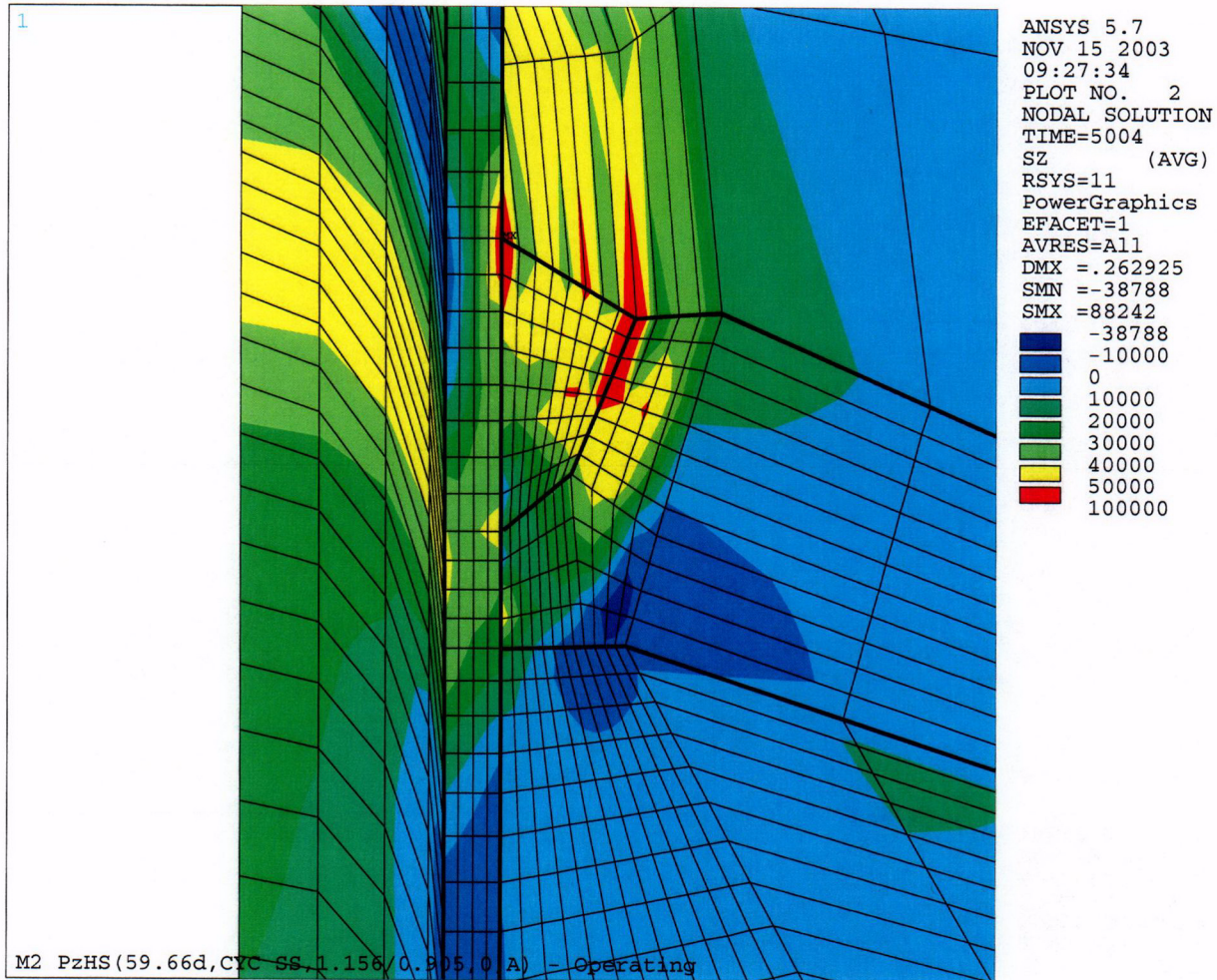


**Figure 5-9b: Mid-plane Axial Stresses for the Steady State Condition for the 59.7° Penetration for the Small Diameter Heater Sleeve**

C-04

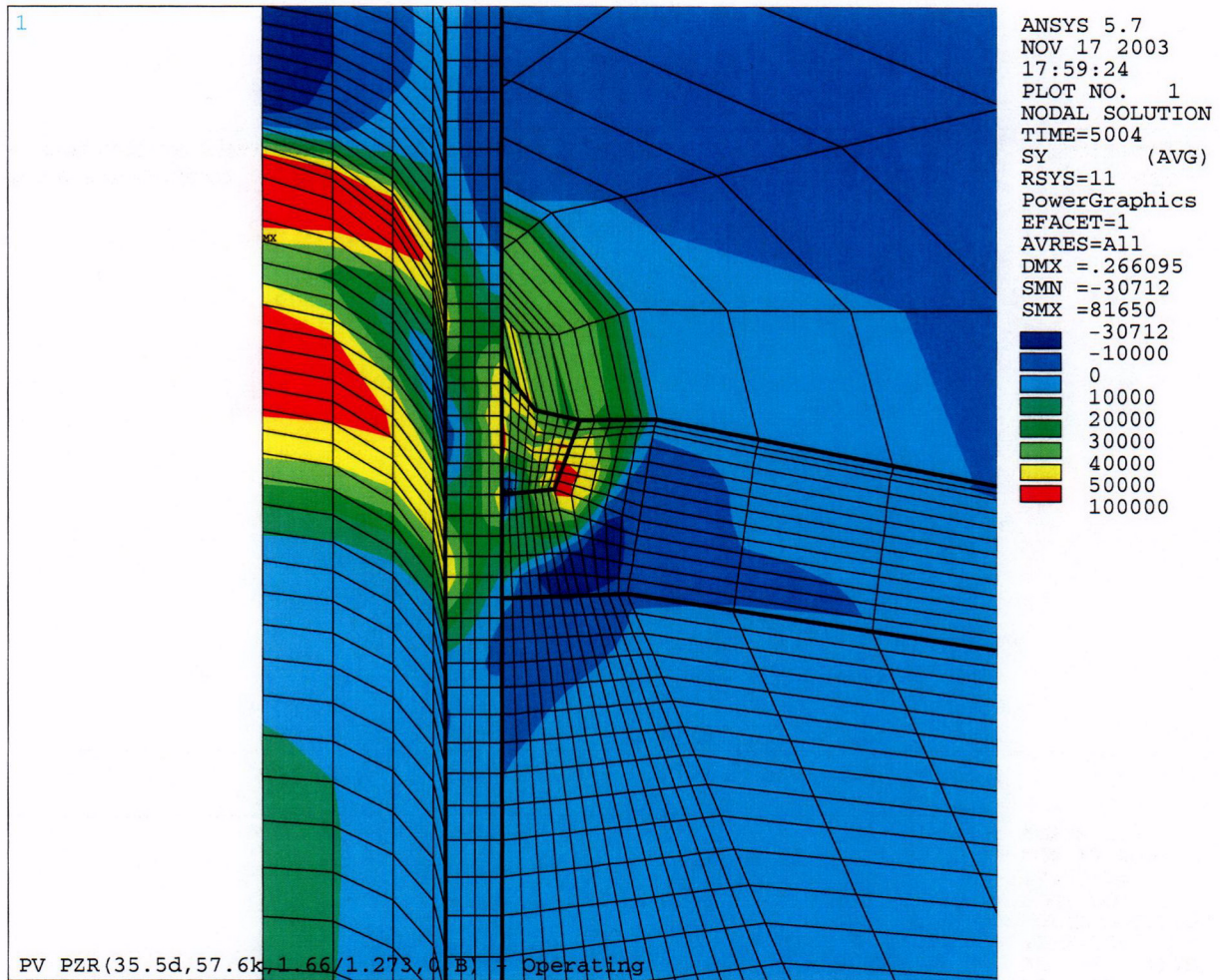


**Figure 5-10a: Mid-plane Hoop Stresses for the Steady State Condition for the 35.5° Penetration for the Large Diameter Heater Sleeve**

C-05

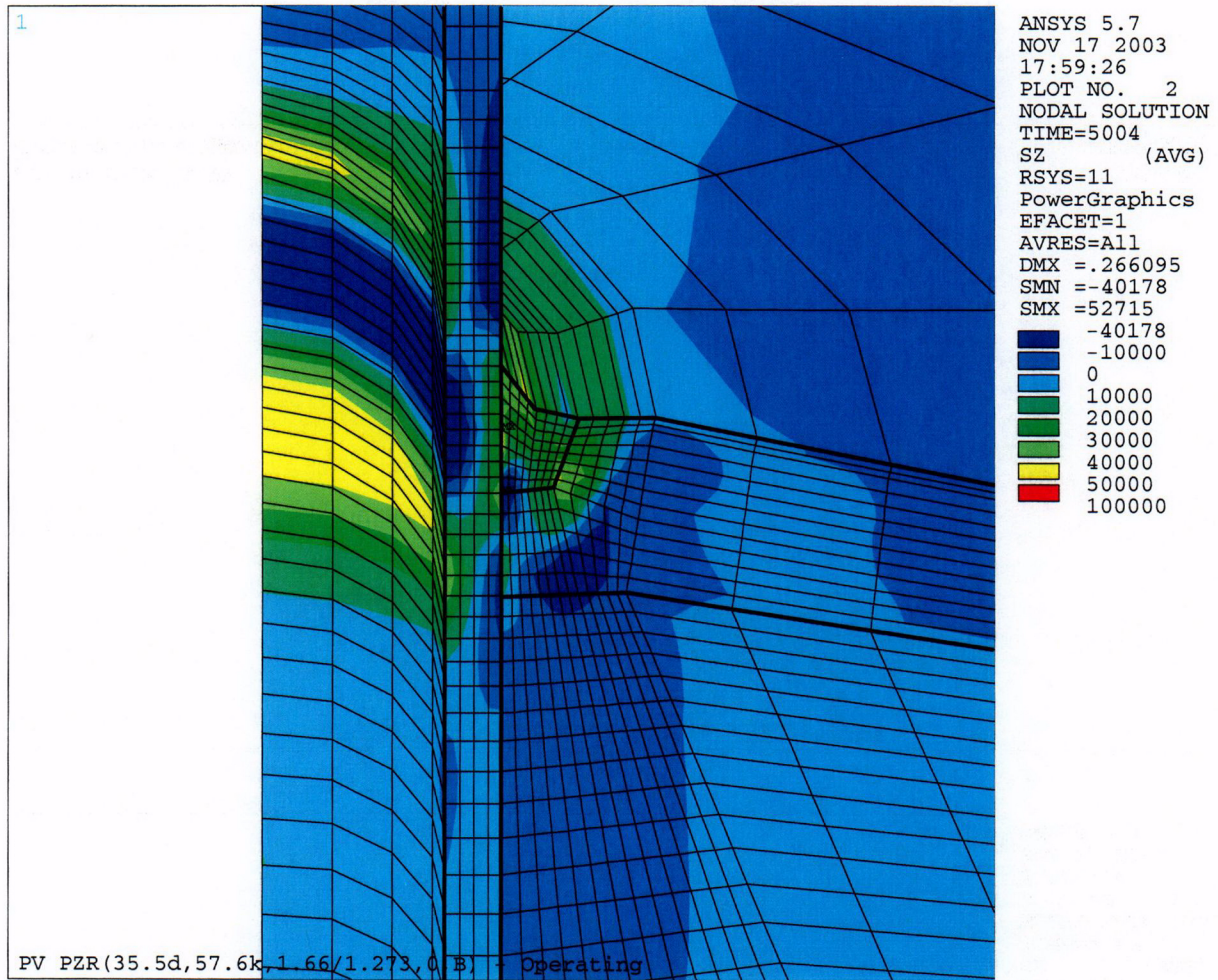


**Figure 5-10b: Mid-plane Axial Stresses for the Steady State Condition for the 35.5° Penetration for the Large Diameter Heater Sleeve**

C-06

### 5.3 FRACTURE MECHANICS ANALYSIS OF THE HEATER SLEEVE

The fracture evaluation was carried out using the approach suggested by the ASME Section XI Appendix C (Reference 15). A range of flaws, including a through-wall circumferential flaw, was postulated to exist in the heater sleeves near the attachment welds.

#### 5.3.1 STRESS INTENSITY FACTOR CALCULATIONS

After the completion of the welding residual stress analysis, which is described in Section 5.2 above, a series of finite element models (See Figures 5-11 and 5-12) were generated to calculate crack tip stress intensity factors for through-wall circumferential cracks at the operating conditions in the presence of welding residual stresses (References 22, 24).

The stresses calculated in the detailed finite element analyses were used to interpolate for the detailed distribution of stresses through the sleeve wall thickness and the circumference for the fracture mechanics calculations using a quadratic interpolation rule.

Cracks of increasing length were analyzed for models with a crack at the bottom of the weld, as well as at 0.25 and 0.5 inches below the bottom of the weld. Cracks above the weld were not considered because the weld was assumed to be intact for these analyses and leakage will not occur.

Each of these cases was analyzed for a crack centered at the uphill and downhill planes of the nozzle. A total of eight crack lengths were analyzed for each model variation: 30°, 80°, 130°, 180°, 220°, 260°, 300°, and 330°. The crack tip stress intensity was evaluated at eight evenly spaced locations through the sleeve wall thickness.

Although the welding residual stress model uses non-linear material strain-hardening properties, the structural model is converted to a fully elastic model for the fracture mechanics analyses. This is appropriate since the correlations for PWSCC crack growth rate are currently provided as a function of the stress intensity,  $K_I$ , which presumes linear elastic fracture mechanics (LEFM).

Operating temperature and pressure were applied to each model case starting from the post-hydrostatic test welding residual stress state, including full operating pressure on the entire crack face. Maximum stresses for representative cases were checked to ensure that the stresses did not exceed reasonable levels for elastic material assumptions outside the crack tip region.

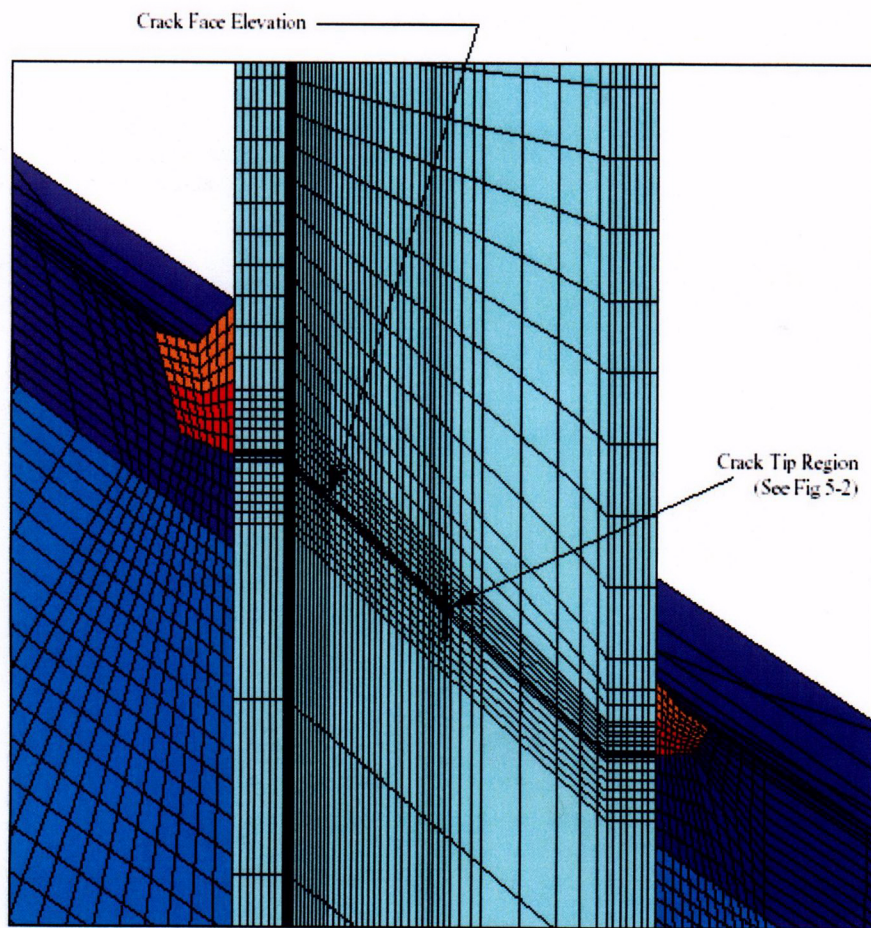


**Figure 5-11: Fracture Mechanics FEM Model – 180° Uphill Centered Circumferential Through-Wall Crack**

C-07

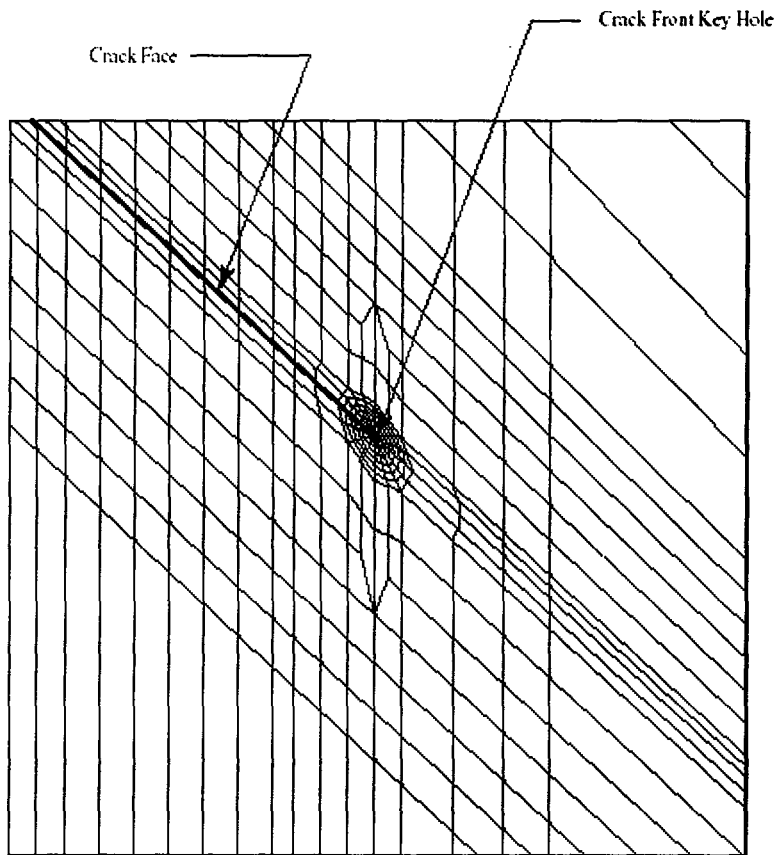


**Figure 5-12: Mesh Details at the Crack Tip**

For the fracture mechanics analyses performed in this calculation, the welding residual stresses were applied as secondary stresses, which redistribute in the presence of the crack. Only the operating pressure is applied as a primary load to the model, both at the model inside and outside diameter wetted surfaces and on the crack face. This is a more accurate approach to modeling the stress state of the cracked nozzle than methods such as superposition.

Calculation of the J-integral values at each of the eight points along the crack front through the wall of the nozzle was performed using software developed by Dominion Engineering. Verification and validation of this software is discussed in Reference 14. The software reads the elastic strain at the crack front elements from the ANSYS (Reference 16) results file and performs the J-Integral value calculations using a numeric volume integration routine. As an output, the software reports the J-integral value as a function of distance along the crack face. Using the relationship between J-Integral and K for the special case of linear elastic materials and using plane strain conditions, the crack tip stress intensity is calculated from the J-integral values with the following equation:

$$K = \sqrt{\frac{J \times E}{1 - \nu^2}} \quad [5-1]$$

where,

K = crack tip stress intensity (psi $\sqrt$ in)

J = calculated J-integral value (psi $\cdot$ in)

E = modulus of elasticity at 650°F = 28.3 x 10<sup>6</sup> psi

$\nu$  = Poisson's ratio = 0.29

The J-integral value calculated by the software is the combined result of fracture Modes I, II, and III loading. Therefore, the value for K calculated using Equation 5-1 is an "equivalent" K that is higher than the K associated with any individual loading mode.

When average crack tip stress intensity is desired, the average of the J-integral values is taken for the entire crack front, then the average J-Integral is converted to the equivalent crack tip stress intensity using Equation 5-1.

The crack tip J-integral was calculated as a function of through-wall depth for the cases described above. From these results, the average through-wall stress intensity and the peak stress intensity were determined. Plots of the average and peak stress intensity factor as a function of crack length for each crack plane elevation considered are included in Figures 5-13 and 5-14 for downhill-centered cracks and in Figures 5-15 and 5-16 for uphill-centered cracks.

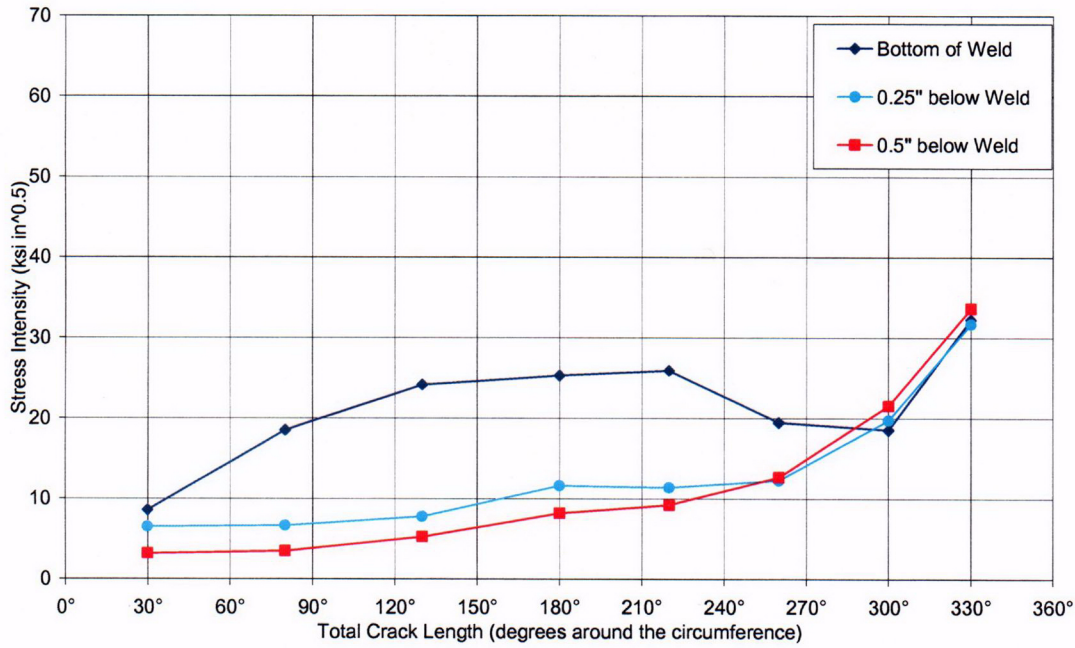


**Figure 5-13: Average Crack Tip Stress Intensity Factor for Downhill-Centered Through-Wall Circumferential Cracks.**

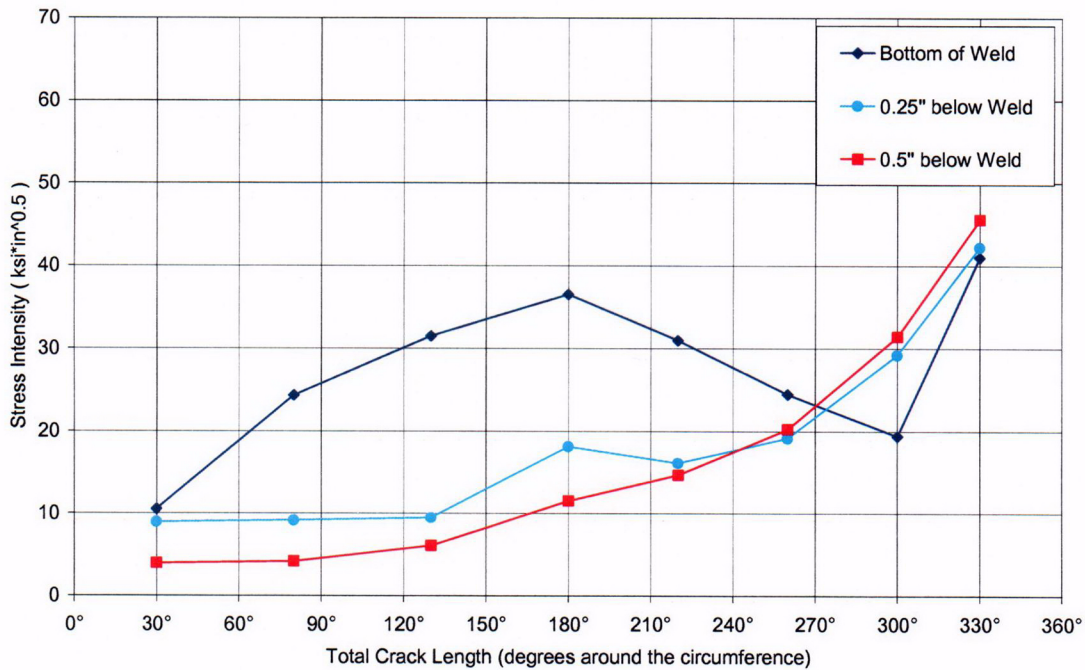


**Figure 5-14: Peak Crack Tip Stress Intensity Factor for Downhill-Centered Through-Wall Circumferential Cracks.**

C-08

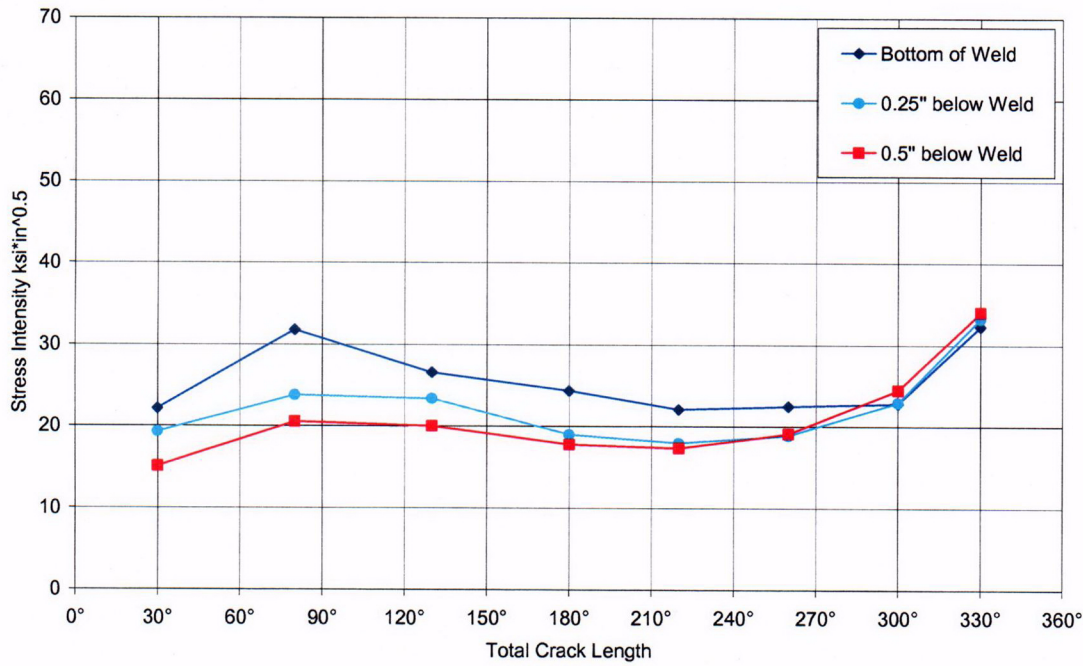


**Figure 5-15: Average Crack Tip Stress Intensity Factor for Uphill-Centered Through-Wall Circumferential Cracks.**

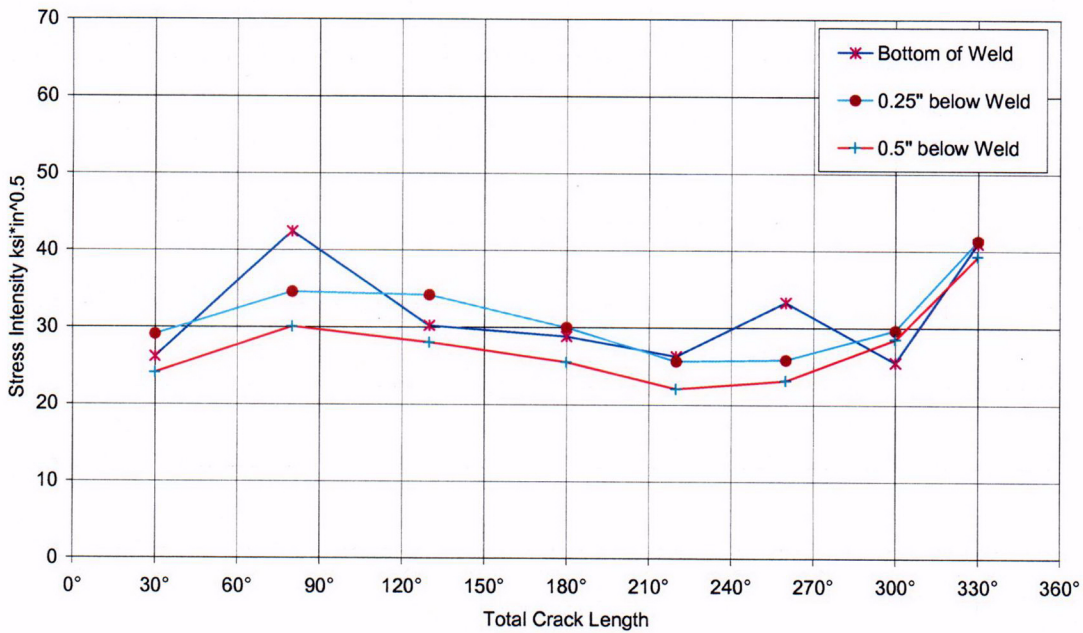


**Figure 5-16: Peak Crack Tip Stress Intensity Factor for Uphill-Centered Through-Wall Circumferential Cracks.**

C-09

#### 5.4 FRACTURE TOUGHNESS AND CRITICAL FLAW SIZE

The other key element in a fracture evaluation is the fracture toughness of the material. The fracture toughness for the Inconel alloy used in the heater sleeve tubes has been taken directly from work by Brown and Mills [Reference 17], because reference values are not yet available in ASME Code Section XI for Ni-Cr-Fe alloys. The fracture toughness for the Alloy 600 is at least equivalent to that of Type 304 or 316 stainless steel, which guarantees that any possible failure will be by ductile limit load.

The allowable flaw size was determined for a circumferential through-wall flaw, using a ductile limit load calculation, following the guidelines of Section XI. Since Section XI Appendix C does not contain calculation methods for through-wall flaws, the equations of Appendix C were modified to cover this case. The maximum pressure was assumed to be 2250 psia.

The only applicable stresses for the determination of the critical flaw length are the pressure stresses at steady state, because thermal stresses do not affect the plastic instability of a ductile component. Also, because the pressurizer skirt is not insulated, there may be some mechanical effect of the temperature difference on the stresses in the bottom head. This was judged to be negligible and was ignored in the determination of the critical flaw length.

The calculations indicate that the critical flaw length is 320° for a circumferential through-wall flaw in a large diameter heater sleeve. For the small diameter heater sleeves, the critical length is 322° (References 22, 25).

#### 5.5 CRACK GROWTH PREDICTIONS

The cracks in the heater sleeves are assumed to be the result of primary water stress corrosion cracking in the Alloy 600 base metal. There are a number of available measurements of static load crack growth rates in primary water environments for Alloy 600. In this section, the available data are compared and a representative growth rate established.

A complete assessment of the future growth of a flaw in one of the heater sleeves would involve consideration of both fatigue crack growth and stress corrosion crack growth. For the time periods considered in this report, the amount of fatigue crack growth is negligible compared to the high stress corrosion crack growth rate resulting from the high temperature.

Efforts to develop crack growth rate models for Alloy 600 have been associated with the initial events of PWSCC of reactor vessel head nozzles. The initial model was that of Scott (Reference 18) who used data from specimens machined from flattened steam generator tubes that were tested in environments typical of PWR primary environments (Reference 19) to develop a crack growth rate model. For data obtained at 626°F (330°C) and corrected for the effects of cold-work from flattening the tubes, Scott's model became

$$\frac{da}{dt} = 2.8 \times 10^{-12} (K - 9)^{1.16} \text{ m / sec} \quad (5-2)$$

Equation 5-2 ultimately was the basis for the PWR Materials Reliability Program (MRP) recommended crack growth rate curve for the evaluation of SCC growth when a power-law dependence on stress intensity factor ( $K_I$ ) was assumed. This report uses the MRP curve for assessing the primary water stress corrosion crack growth rate in Alloy 600. The following paragraphs briefly describe the development of the MRP curve.

Subsequent to the development of the Scott relationship, several laboratories conducted stress corrosion crack growth rate studies in simulated primary water of Alloy 600 typical of that used in CRDM nozzles. These laboratories included Westinghouse, EDF, Framatome, CEA, Studsvik, and Ciemat (References 20A-20K). An independent panel formed by MRP reviewed the available stress corrosion crack growth data, comparing the data against a set of stringent screening criteria for use in developing the crack growth rate curve. The test results considered in the development of the MRP crack growth rate curve were from tests performed in controlled simulated primary coolant environments using fracture mechanics specimens. The testing had careful control of applied load (stress intensity factor,  $K_I$ ) and temperature and had accurate measurements of crack growth rates. The crack growth rates in these tests were based on average lengths to the stress corrosion crack front. All of the data were from tests in the range of 554°F (290°C) to 686°F (363°C) to minimize the adjustment to account for differences in test temperatures.

A total of 158 data points survived the screening criteria. These data were then used by the MRP panel to develop a stress corrosion crack growth curve for Alloy 600. There is a general agreement that crack growth in Alloy 600 in the primary water environment can be modeled using a power-law dependence on stress intensity factor with differences in temperature accounted for by an activation energy (Arrhenius) model for thermally controlled processes.

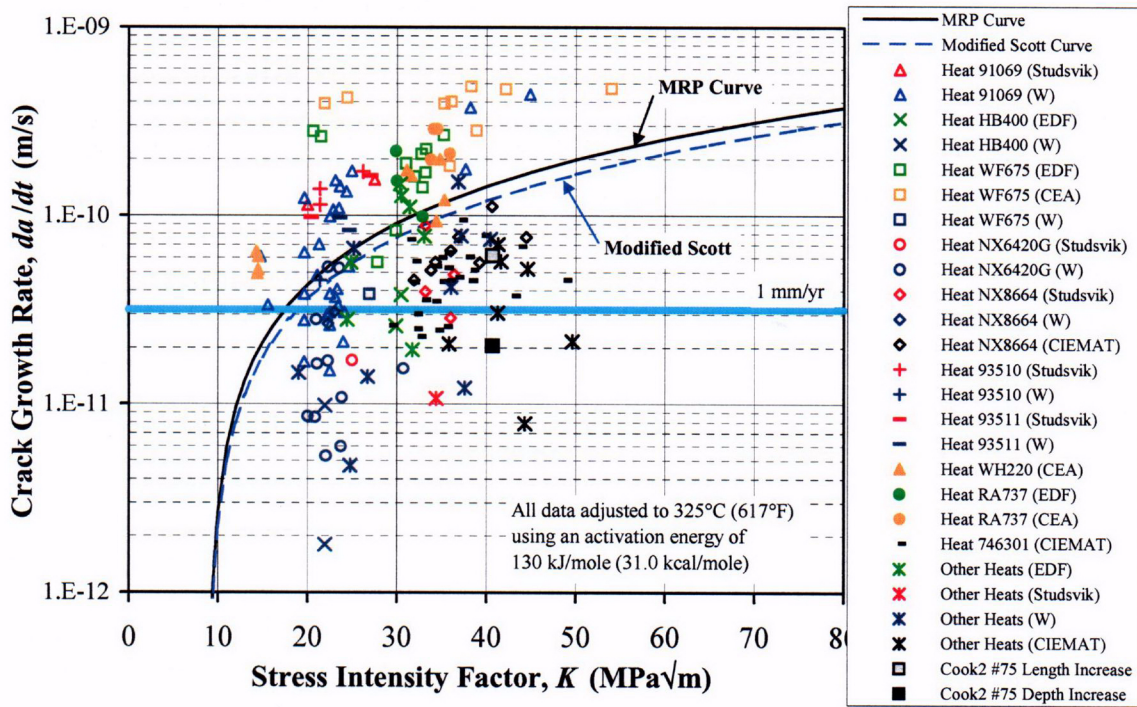


**Figure 5-17: Screened Laboratory Data for Alloy 600 with the MRP Recommended Curve. The Modified Scott Model is also Shown**

The recommended mean curve shown in Figure 5-17 was determined by linearized least-squares fit to the temperature-adjusted CGR data in Figure 5-17 using the power-law relationship:

$$CGR = \dot{a} = \alpha(K - K_{th})^\beta \tag{5-3}$$

where:

- $\dot{a}$  = crack growth rate
- $\alpha$  = crack growth amplitude
- $K$  = crack tip stress intensity factor
- $K_{th}$  = crack tip stress intensity factor threshold
- = 9 MPa  $\sqrt{m}$  (8.2 ksi  $\sqrt{in}$ )

C-10

$\beta$  = exponent on stress

The function minimized by the linearized least-squares fit for each heat of material is  $f(\alpha, \beta)$  where:

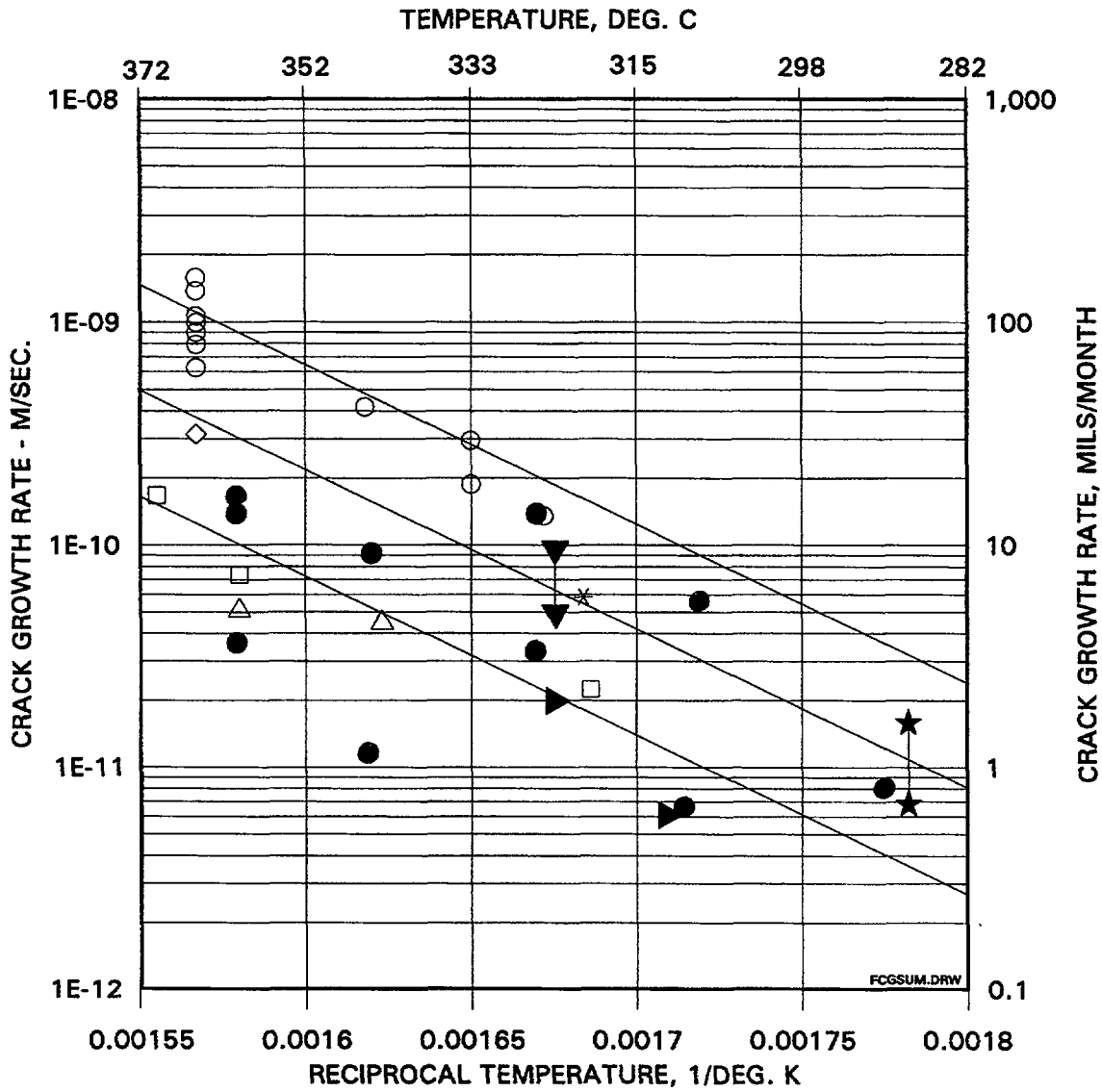
$$f(\alpha, \beta) = \sum_{i=1}^n \{ \ln(\dot{a}_i) - [\ln(\alpha) + \beta \ln(K_i - 9)] \}^2 \quad (5-4)$$

and  $n$  is number of test data points in each heat of material. The same procedures were repeated for all 26 heats for which the test data are available [Reference 21]. This results in 26 individual  $\alpha$ -values, assuming a single given value of  $\beta = 1.16$  applicable for all heats. The most representative  $\alpha$ -value suitable for stress corrosion cracking evaluation was then determined based on the statistical aspects of the data, which are discussed in the following paragraphs. The value for the crack tip stress intensity factor threshold  $K_{th}$  is taken as  $9 \text{ MPa}\sqrt{\text{m}}$  in accordance with previous practice [Reference 20A].

The MRP crack growth curve was structured to bound 75 percent of the 26 heats for which test results were available. Fits were done on the results for each heat, and the constant term was determined for each heat. This was done to eliminate the concern that the curve might be biased from a large number of results from a single heat. The 75<sup>th</sup> percentile was then determined from these results. The MRP panel on crack growth endorsed the resulting curve unanimously in a meeting on March 6<sup>th</sup> and 7<sup>th</sup> 2002. This approach is consistent with the ASME Code Section XI flaw evaluation philosophy, which is to make a best estimate prediction of future growth of a flaw. Margins are incorporated in the allowable flaw sizes. The entire data set is shown in Figure 5-17, where the data have been adjusted to a single temperature of 617°F (325°C).

Since the CE pressurizers operate at a temperature of 653°F (345°F) or 643°F (339°C), and the crack growth rate is strongly affected by temperature, a temperature adjustment was necessary. The temperature correction was obtained from study of both laboratory and field data for stress corrosion crack growth rates for Alloy 600 in primary water environments. The available data showing the effect of temperature are summarized in Figure 5-18. Most of the results shown here are from steam generator tube materials, with several sets of data from operating plants, and results from two heats of reactor vessel head nozzle materials tested in a laboratory [Reference 20A].

Analysis of the data shown in Figure 5-18 results in an activation energy of 31-33 Kcal/mole, which was used to adjust for the different operating temperature. This value is slightly lower than the generally accepted activation energy of 44-50 Kcal/mole used to characterize the effect of temperature on crack initiation.



Note: All symbols are for steam generator tube materials, except for the solid circles, which are head penetration laboratory data

**Figure 5-18: Summary of Temperature Effects on PWSCC Growth Rates for Alloy 600 in Primary Water**

Considering the requirement to account for temperature when applying the mean curve, the provisional recommended growth curve for PWSCC of Alloy 600 materials is as follows:

$$\dot{a} = \exp \left[ -\frac{Q_g}{R} \left( \frac{1}{T} - \frac{1}{T_{ref}} \right) \right] \alpha (K - K_{th})^\beta \quad (5-5)$$

where:

$\dot{a}$  = crack growth rate in m/s

$Q_g$  = thermal activation energy for crack growth

= 130 kJ/mole (31.0 kcal/mole)

$R$  = universal gas constant

=  $8.314 \times 10^{-3}$  kJ/mole °K ( $1.103 \times 10^{-3}$  kcal/mole-°R)

$T$  = absolute operating temperature at location of crack (°K or °R)

$T_{ref}$  = absolute reference temperature used to normalize data

= 598.15°K (1076.67°R)

$\alpha$  = crack growth amplitude

=  $6.22 \times 10^{-12}$  at 345°C (653°F)

$K$  = crack tip stress intensity factor ( $\text{MPa}\sqrt{\text{m}}$ )

$K_{th}$  = crack tip stress intensity factor threshold

=  $9 \text{ MPa}\sqrt{\text{m}}$

$\beta$  = exponent, assumed as 1.16

Use of the 31 Kcal/mole activation energy results in the need for a correction factor for crack growth rates in the heater sleeves with a pressurizer head temperature of 345°C (653°F). Use of a correction for 653°F will be conservative for the two CE plants which currently have pressurizer operating temperatures of 643°F. Therefore the following crack growth rate model was used for the heater sleeves for crack growth in all the cases analyzed.

$$\frac{da}{dt} = 6.22 \times 10^{-12} (K - 9)^{1.16} \text{ m/sec}$$

where:

$$K = \text{applied stress intensity factor, in MPa}\sqrt{\text{m}}$$

Reference 21 recommends that a factor of 2 be applied for the calculation of stress corrosion crack growth for circumferential flaws in reactor vessel upper head nozzles. This results from the potential for PWR primary coolant to accumulate in the annulus between the nozzle and the low alloy steel head material. If this were to happen, the lithium in the primary coolant could concentrate slightly, producing a mildly alkaline environment. There are data which indicate a slight elevation of Alloy 600 PWSCC crack growth rates under these conditions. For the heater sleeves, the circumferential cracking will be ID initiated and there is no mechanism for concentration of the lithium in the coolant. Once leakage into the annulus between the heater sleeves and pressurizer bottom head develops, concentration of the lithium is more difficult because the annulus is more open than the reactor vessel head nozzle situation where an interference fit exists at room temperature. For these reasons, the factor of 2 on circumferential crack growth rates was not applied.

## 5.6 LEAK RATE CALCULATIONS

Parametric leakage rate calculations were performed for the hypothetical circumferential flaws in the pressurizer heater sleeves for CE nuclear plants.

For the two different heater sleeve sizes, leakage rates were computed for various through-wall circumferential flaws using the steady state normal operating pressure loads. Calculations were performed in two steps: first, estimation of the crack opening areas for various assumed circumferential through-wall crack lengths from the sleeve geometry, loading and the material properties followed by leak rate predictions as a function of these crack opening areas. Two-phase flow and the crack surface roughness were considered in the calculations. Material Properties for Inconel alloy SB-167 (N06600 alloy) were taken from ASME Code Section II Part D.

Procedures used in these calculations have been reviewed and approved by the NRC in prior work for Leak-before-Break (LBB) reports on reactor primary loop systems, for example, Reference 26. Using the results of the leak rate calculations, plots were generated providing the leak rate as a function of flaw size in Fig.5-19 for the large diameter sleeves and in Fig.5-20 for the small diameter sleeves.

The leakage rate assessments showed that the circumferential through-wall flaws in the heater sleeves for two different sizes used in the CE fleet of pressurizers are in the range of 0.3 to 0.5 gallons per minute for the flaws that extend approximately 1/3 of the circumference of the tubes. It is important to realize that much smaller through-wall flaws will result in boric acid deposits on the bottom head of the pressurizer.

By comparing the critical through-wall circumferential flaw sizes for the heater tube sleeves with those resulting in the detectable leakage, the margins between the flaws with detectable leakage and the critical flaw lengths that lead to ejection of the sleeves is large.

The RCS pressure boundary required leak detection capability for the plants is 1 gpm. However, the actual capability is closer to 0.1 gpm. All plants monitor their leakage rates constantly, and are very sensitive to departures from average leak rates. Typically, even small departures from the average unidentified leak rates are investigated.

A specific leak rate criterion is not required for the pressurizer heater sleeves for two reasons. First, the leakage rates necessary to show the visual evidence of boron deposits on the pressurizer bottom head is much lower than the technical specification limit. Second, all plants have significantly increased their sensitivity to leakage monitoring in the past two years in response to the Davis Besse incident. Very small changes in the unidentified leakages at the base of the pressurizer are carefully investigated.

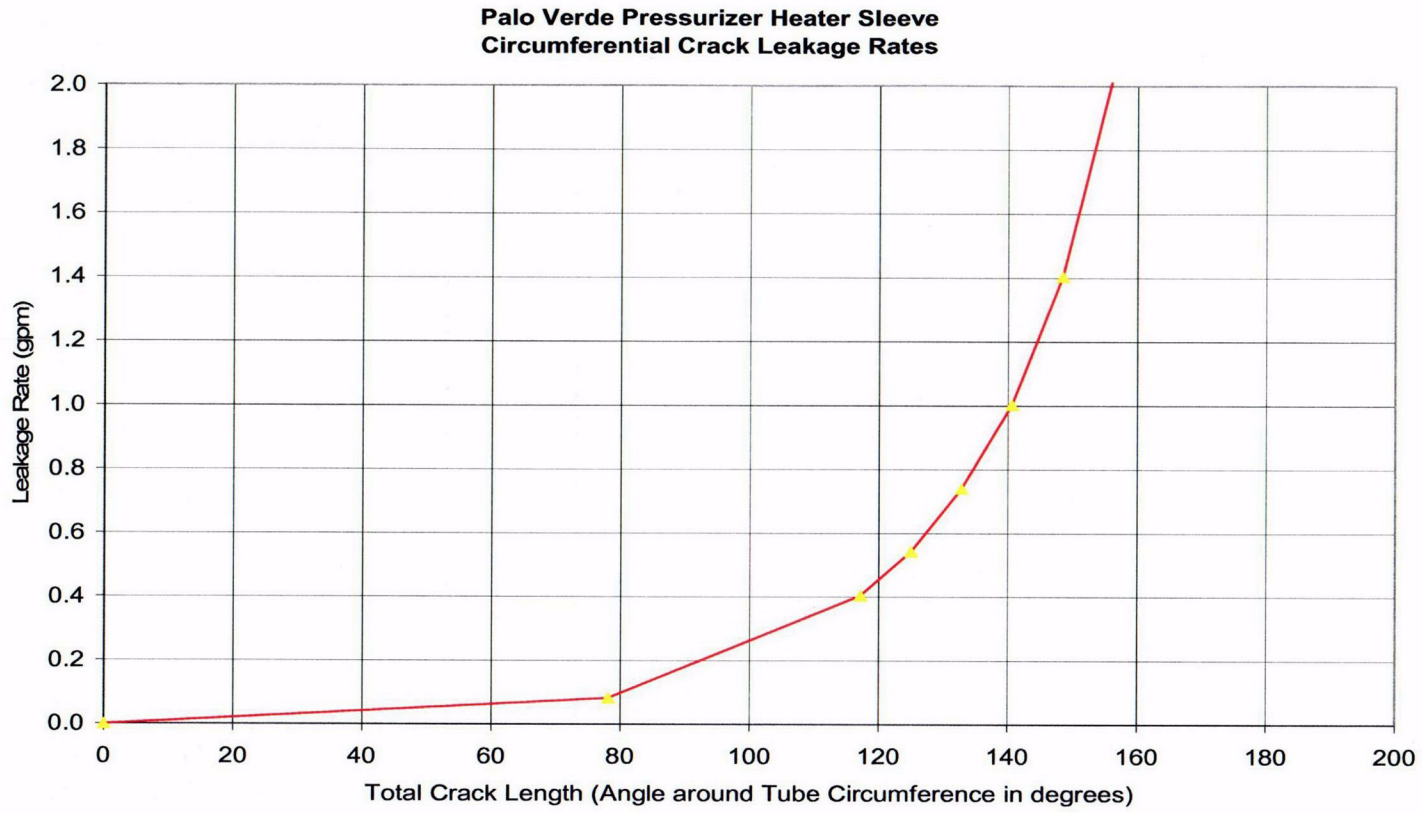


**Figure 5-19: Leak Rate vs Flaw Size for Large Diameter Heater Sleeves**

C-11

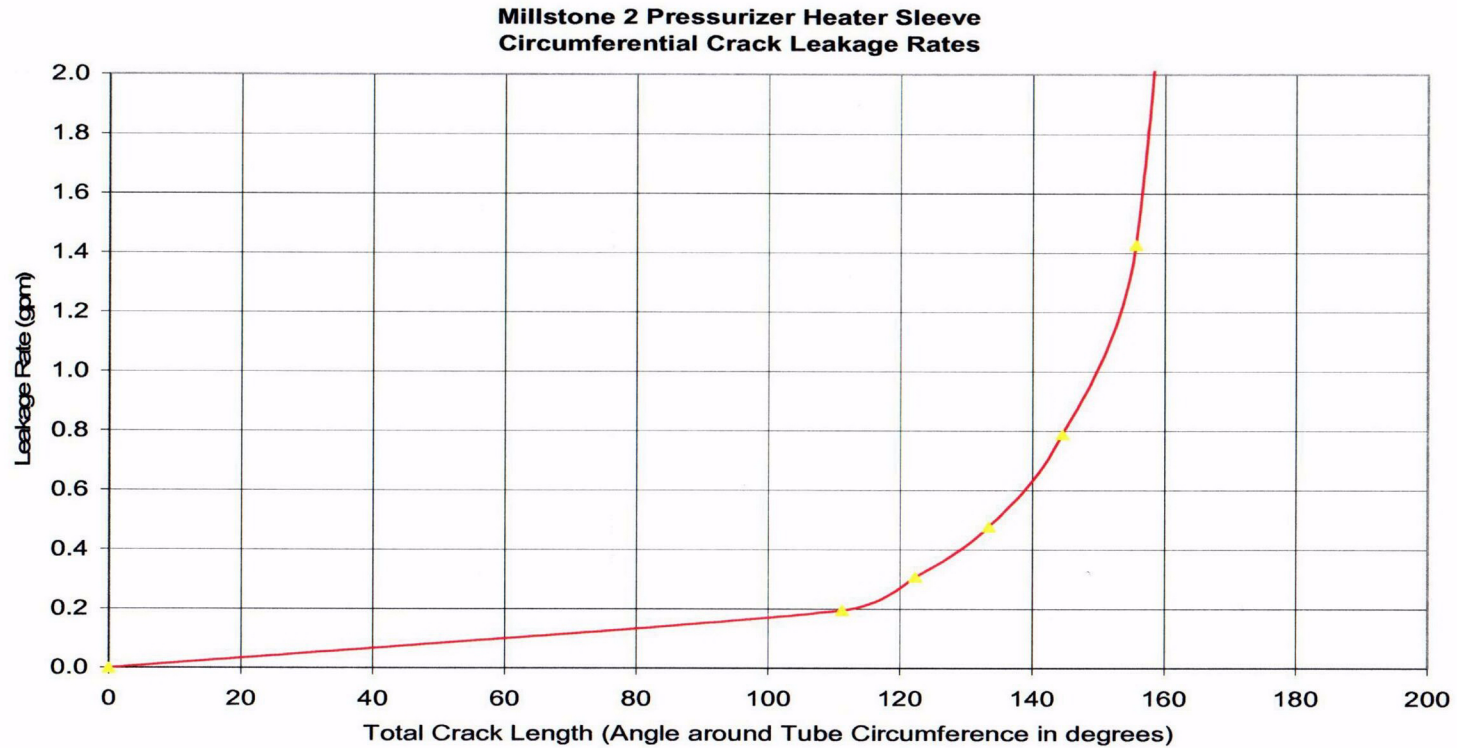


**Figure 5-20: Leak Rate vs Flaw Size, Small Diameter Heater Sleeves**

C-12

## 5.7 TIME FOR PROPAGATION FROM LEAK TO CRITICAL FLAW SIZE

Separate analyses were completed for the small diameter and the large diameter heater sleeves. In each case, the stress analysis was used as input to the crack growth calculation, which provided the time to grow to the critical flaw length. The leak rate calculations were used to ensure that leakage from the starting flaw size would be detectable either as boron deposits or by the plant leakage detection system.

**Small Diameter Sleeves.** Of the three different sleeve locations, the outermost sleeve is the governing location. A through-wall flaw was postulated at the highest stress location, just below the J-groove weld, with an initial length of 30 degrees. The crack growth was calculated for this flaw, and the results are shown in Figure 5-21. The results show that a through-wall flaw is predicted to grow from a 30 degree flaw to a critical length in approximately ten years. Additional time would be required to grow the flaw to the 30 degree condition. Although the leak rate for flaws of less than 30 degrees extent is relatively small, such leak rates are sufficient to leave significant boric acid deposits on the bottom head to be visible during visual inspections. The next aspect of the evaluation was to determine the leakage to be expected from a circumferential flaw with a length equal to the assumed length of one third the circumference, or 120 degrees. Figure 5-20 shows that such a flaw would yield leakage of approximately 0.3 gpm, which is enough to produce visible boron, and probably sufficient to ensure detection by the plant leak detection system. Figure 5-21 indicates that the time for a 120° flaw to the critical size for failure was 7.8 years.

**Large Diameter sleeves.** Again, comparison of the stresses for the three sleeve location shows that the outermost sleeve is governing, but because only a few plants have sleeves in a third row, a survey was done of those plants, and the highest yield strength was chosen, at 48.5 ksi. The crack growth results for the outermost sleeve are shown in Figure 5-22. The maximum yield strength in the plants for the inner two rows are higher, at 57 ksi, than for the sleeves in the third row. The results for these inner row sleeves with higher yield strengths show that the crack growth is actually higher, as seen in Figure 5-23. The governing time to failure for the larger diameter sleeves is shown in Figure 5-23, and is ten years to grow from a 30 degree flaw. Again, considering the leak rate calculations for the large diameter sleeves, a through-wall flaw with a length of 120 degrees will give a leak rate of approximately 0.5 GPM, as shown in Figure 5-19. Figures 5-22 and 5-23 indicate that the times to grow from a 120° flaw to the critical flaw size is 13.2 years for the outermost sleeves and 7.5 years for the sleeves at the 35.5° location. For the larger sleeves, the 35.5° location is governing.

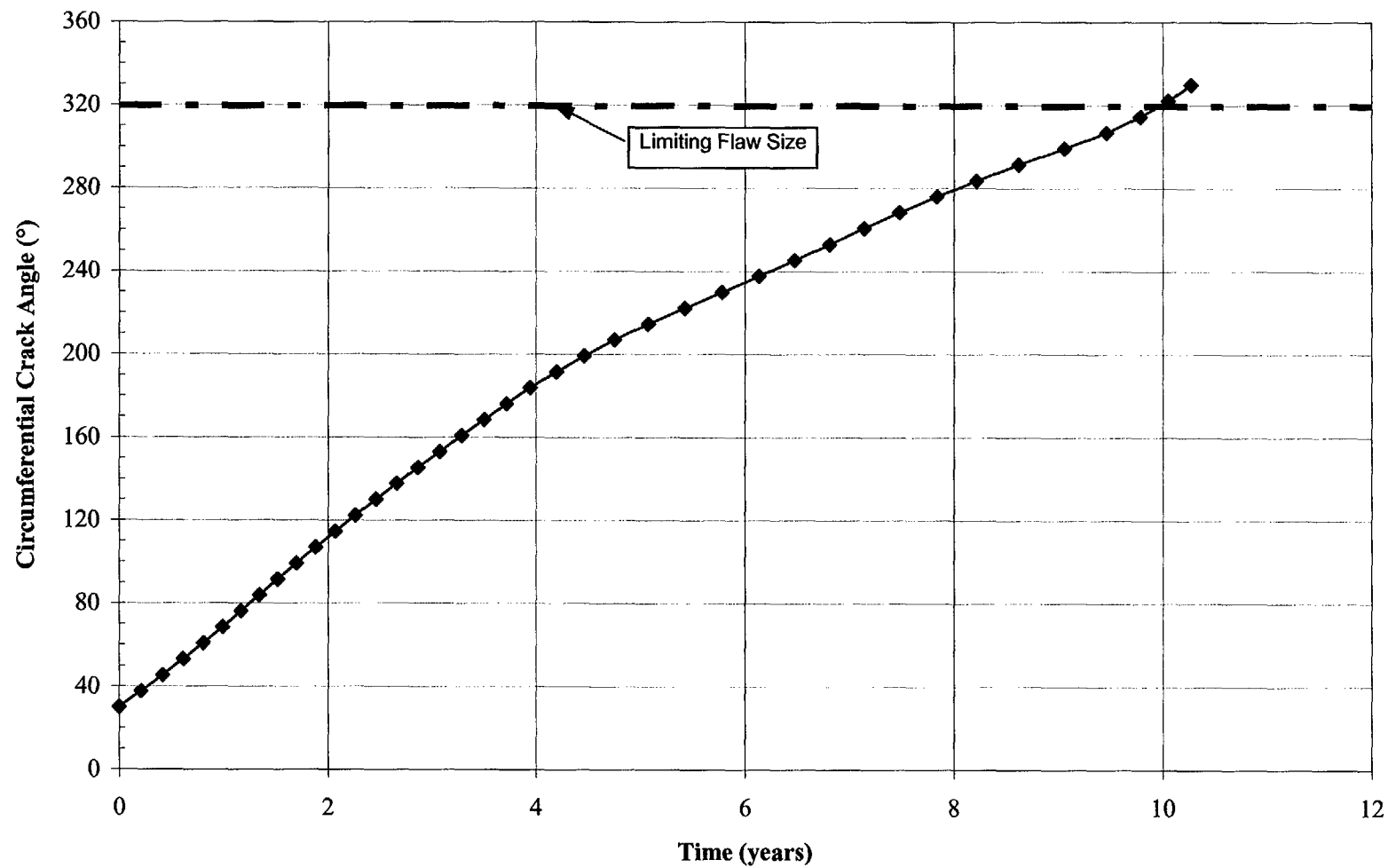


Figure 5-21: Circumferential Crack Length versus Time for 59.7° Small Heater Sleeves

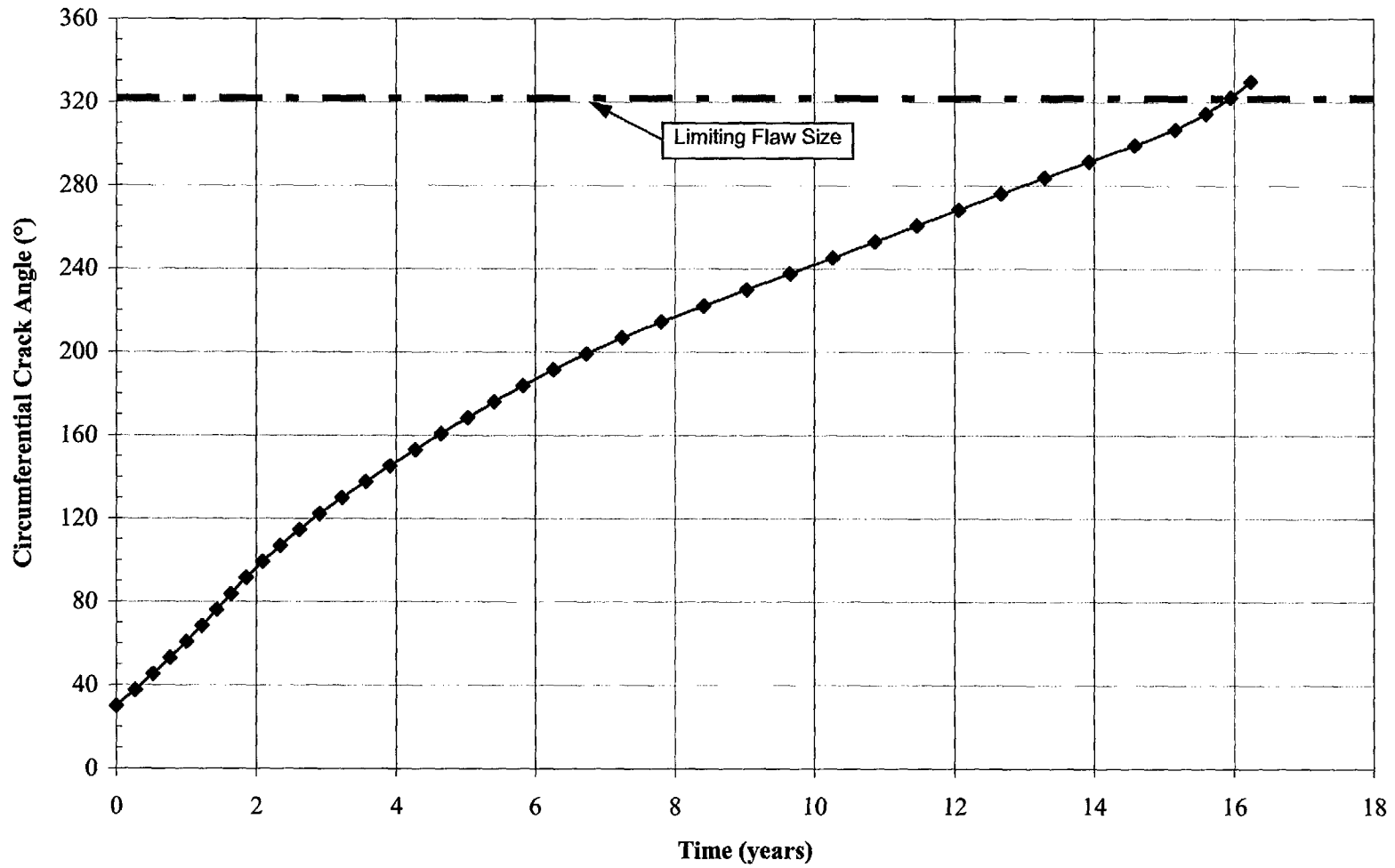


Figure 5-22: Circumferential Crack Length versus Time for 52.0° Large Heater Sleeves

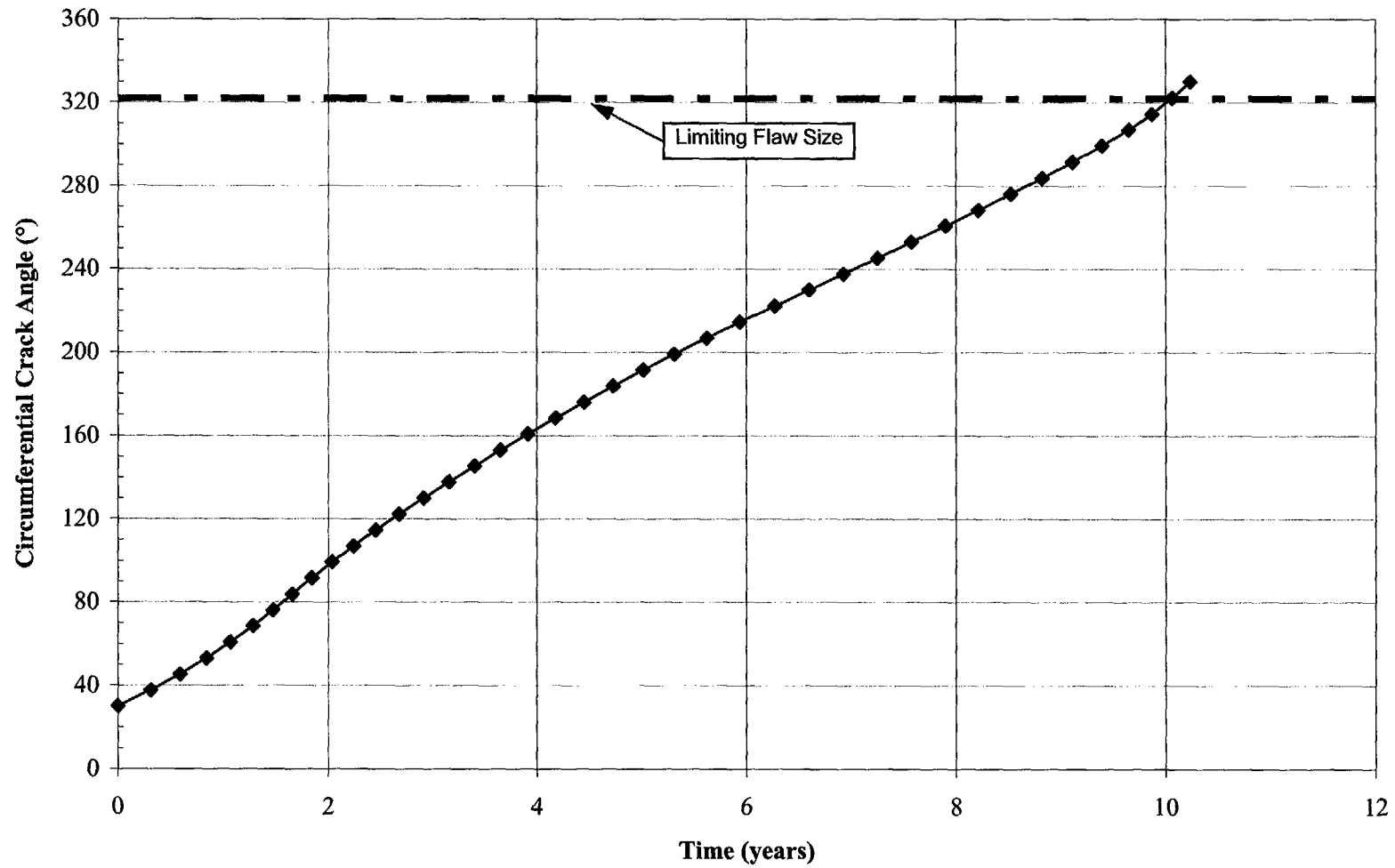


Figure 5-23: Circumferential Crack Length versus Time for 35.5° Large Heater Sleeves

## 6 SUMMARY AND CONCLUSIONS

The reviews and calculations described in the preceding sections resulted in the following conclusions and findings about the Palo Verde-2 pressurizer heater sleeve circumferential flaws and their significance to the other CE design units which have not replaced their heater sleeves and taken other mitigative actions to reduce the potential for PWSCC initiation.

To evaluate the integrity of the heater sleeves, through-wall circumferential flaws were postulated to exist in the high stress region just below the J-groove attachment weld. This assumption is conservative for a number of reasons. No such flaws have been detected in operating plants (the Palo Verde-2 flaws were inboard of the welds). The stresses vary significantly around the circumference of the sleeves, thus the flaws would likely initiate only in a few areas of high stress. A more realistic flaw might be a part-through-wall circumferential flaw, but such a flaw would have to extend continuously around the sleeve and have a depth exceeding 80 to 90 % of wall thickness to cause a sleeve ejection. Such a flaw is extremely unlikely without the flaw breaking through to cause a leak because of the stress variation around the circumference. Axial flaws were not considered because they are not a threat to cause ejection.

The heater sleeve integrity evaluation for the large sleeves indicated that at least 10 years would be required for a flaw which provides detected leakage (30° circumferential extent) to propagate to the critical size for sleeve ejection. If the criterion is a detectable leakage rate, assumed in this evaluation to be 0.5 gpm, then the time to grow to critical flaw size is at least 7.5 years. These times are applicable for all large diameter sleeves regardless of location. The analysis supporting this conclusion considered the combination of highest hillside location and the highest yield strength sleeves (48.5 KSI) present in any plant with sleeves at this angle. Crack growth was higher for the outermost sleeves at Palo Verde-2 (and Palo Verde-1 and -3) which are at a smaller angle (35.5°) but have significantly higher yield strength (57 KSI) Alloy 600.

For the small diameter heater sleeves, the most limiting location is the outermost (highest angle) location. Considering the most limiting yield strength and the highest stress location (just below the J-weld), a 30° circumferentially oriented flaw will also require 10 years to grow to the critical flaw size for sleeve ejection. If the alternate criterion of a detectable leak rate is used, at least 7.8 years will be required to propagate a flaw to critical size.

Based on the calculated times to sleeve ejection from a flaw size with detectable leakage, the presently implemented visual inspection program for the pressurizer bottom head region will be sufficient to insure the integrity of the pressurizer.

The mechanism causing the flaws cannot be determined based on the NDE results. However, numerous other Alloy 600 heater sleeves and small diameter nozzles have developed through-wall and part through-wall cracks in service. Several destructive examinations of leaking heater sleeves and nozzles indicate that PWSCC was the likely cause of these flaws. Alloy 600, when highly stressed in high temperature water is susceptible to PWSCC. The Palo Verde-2 flaws are assumed to be another example of PWSCC.

The NDE indications at Palo Verde-2 are circumferentially oriented flaws above the partial penetration welds in the Alloy 600 heater sleeves, and are not in the pressure boundary. Thus, should the through-

wall circumferential extent of the flaws exceed the critical flaw size, the heater sleeves cannot be ejected nor will the flaws leak primary coolant to the pressurizer OD surface. Similarly, the two axial flaws examined were not in the pressure boundary and would not leak.

The circumferential orientation of the flaws indicates high stresses in the axial direction. This indicates that stresses other than normal operating stresses and weld residual stresses may have initiated and propagated the flaws. However, the finite element stress analyses of heater sleeves indicate higher hoop stresses which would result in flaws oriented in the axial direction. The analytical stress analysis results are consistent with field experience. When inspected by various NDE techniques, cracks in heater sleeves and similar small diameter Alloy 600 applications have been oriented in the axial direction.

The Alloy 600 pipe used for the Palo Verde-2 sleeves had relatively high yield strength but the sleeves in other CE units have even higher yield strengths. In pressurizer applications, Alloy 600 with a range of yield strengths has proven to be susceptible to PWSCC. Heats with higher and lower yield strengths have experienced PWSCC. There appeared to be nothing unique about the Palo Verde-2 (and Palo Verde-1 and -3) Alloy 600 other than the Alloy 600 was supplied by B&W Tubular Products. The only units with such materials in the heater sleeves are Palo Verde-1, -2 and -3.

There were not any unique or unusual steps in the sleeve fabrication process that would have made these sleeves more susceptible to PWSCC than sleeves in other CE units nor made the development of circumferentially oriented flaws more likely at Palo Verde-2. All of the Palo Verde-2 sleeves were reamed after installation in the pressurizer to permit heater installation. Reaming would have caused a thin layer of cold-worked material which would have been more susceptible to PWSCC initiation. However, reaming was not unique to PV-2. Such reaming was permitted and was probably performed on many sleeves in other CE plants.

Heater sleeve ejection, should it occur, would be equivalent to a small break LOCA (SBLOCA). The consequences of such a postulated event are bounded by the results of Palo Verde SBLOCA ECCS performance analysis. If a postulated heater sleeve ejection were to occur, the event would be handled by the existing Operator Response and Emergency Procedure Guidance like any other LOCA. The existing guidance provides adequate direction to mitigate the transient. No additional operator guidance is needed to address such an event, should it occur.

A review of the risk assessment of failure (ejection of a sleeve) on overall plant core damage frequency (CDF) and large early release frequency (LERF) concluded that the impact of failure on CDF is bounded by  $8.11E-07$  per year and the incremental LERF due to the postulated failure is less than  $1.0E-08$  per year.

Potential jet impingement/missile damage from a heater ejection event is not increased by the postulated event because of design and location of the pressurizer within the concrete compartment. The design and location of the pressurizer provide protection from the failure of the surge line, which results in a much larger break than a heater sleeve failure. The heater sleeve failure scenario is bounded by the surge line break (much larger break) sub-compartment pressurization analysis. CDF would be within the range of  $4.2E-08$  and  $6.3E-07$  per year and the incremental LERF due to the postulated failure would be between  $4.2E-10$  and  $6.3E-09$ .

## 7 REFERENCES

1. J. F. Hall, D. B. Scott, D. A. Wright, and R. S. Pathania, "Cracking of Alloy 600 Heater Sleeves and Nozzles in PWR Pressurizers", Proceedings of the Fifth International Conference on Environmental Degradation of Materials in Nuclear Power Systems - Water Reactors, American Nuclear Society, 1996, pp652-660.
2. CE NPSD-406, "Failure Analysis of ANO-2 Ruptured Pressurizer Heater and Cracked Sleeve", July 1987.
3. CEN-393-P, "Evaluation of Pressurizer Heater Sleeve Susceptibility to Primary Water Stress Corrosion Cracking", November 1989.
4. CE NPSD-690-P, "Evaluation of Pressurizer Penetrations and Evaluation of Corrosion after Unidentified Leakage Develops CEOG Task 700", January 1992.
5. W. H. Bamford and J. F. Hall, "A Review of Alloy 600 Cracking in Operating Nuclear Power Plants", Proceedings of the Eleventh International Conference on Environmental Degradation of Materials in Nuclear Power Systems - Water Reactors, American Nuclear Society, August 10-14, 2003 (to be published).
6. J. Molkenhuth and J. Hall, "Odd and Unusual Stress Cracking Occurrences in Alloy 600 Components", EPRI Workshop Primary Water Stress Corrosion Cracking of Alloy 600 in PWR's, November 15-17, 1994.
7. CE NPSD-617-P, "Destructive Examination of Pressurizer Instrumentation Nozzles from Calvert Cliffs Unit 2 and Evaluation of Similar Nozzles", February 1991.
8. CE NPSD-646, "CEOG Pressurizer Heater Sleeve Thermal Analysis", May 1991.
9. CE NPSD-659-P, "Additional Pressurizer Heater Sleeve Examinations", September 1991.
10. CE NPSD-648-P, "Corrosion and Corrosion/Erosion testing of Pressurizer Shell Material Exposed to Borated Water", April, 1991.
11. Palo Verde Nuclear Generating Station Units 1, 2, and 3, "Updated Safety Analysis Report," August 2003.
12. Code of Federal Regulations, Title 10, Part 50, Section 50.46, "Acceptance Criteria for Emergency Core Cooling Systems for Light Water Nuclear Power Reactors."
13. Combustion Engineering Emergency Procedure Guidelines, CEN-152, Revision 5.2, November 30, 2001.

14. Broussard, J., and Gross, D., "Welding Residual and Operating Stress Analysis of RPV Top and Bottom Head Nozzles," to be published in proceedings of the NRC Vessel Head Penetration Inspection, Cracking and Repair Conference, September 2003.
15. ASME Boiler and Pressure Vessel Code, 1995 Edition, published by ASME.
16. ANSYS Users' Manual, Volume 1, ANSYS, Inc., Houston, PA, 1994.
17. Mills, W. J. and Brown C. M., "Fracture Toughness of Alloy 600 and EN82H Weld in Air and Water" Report B-T-3264 US Department of Energy, June 1999.
18. Scott, P. M., "An Analysis of Primary Water Stress Corrosion Cracking in PWR Steam Generators," Proceedings, Specialists Meeting on Operating Experience With Steam Generators, Brussels Belgium, Sept. 1991, pages 5, 6.
19. McIlree, A. R., Rebak, R. B., Smialowska, S., "Relationship of Stress Intensity to Crack Growth Rate of Alloy 600 in Primary Water," Proceedings International Symposium Fontevraud II, Vol. 1, p. 258-267, September 10-14, 1990.
- 20A. Crack Growth and Microstructural Characterization of Alloy 600 PWR Vessel Head Penetration Materials, EPRI, Palo Alto, CA. 1997. TR-109136.
- 20B. Vaillant, F. and C. Amzallag. "Crack Growth Rates of Alloy 600 in Primary Water," Presentation to the EPRI-MRP Crack Growth Rate (CGR) Review Team, Lake Tahoe, NV, presented August 10, 2001, and revised October 11, 2001
- 20C. Vaillant, F. and S. Le Hong. Crack Growth Rate Measurements in Primary Water of Pressure Vessel Penetrations in Alloy 600 and Weld Metal 182, EDF, April 1997. HT-44/96/024/A.
- 20D. Framatome laboratory data provided by C. Amzallag (EDF) to MRP Crack Growth Rate Review Team, October 4, 2001 (Proprietary to EDF).
- 20E. Cassagne, T., D. Caron, J. Daret, and Y. Lefevre. "Stress Corrosion Crack Growth Rate Measurements in Alloys 600 and 182 in Primary Water Loops Under Constant Load," Edited by F. P. Ford, S. M. Bruemmer, and G. S. Was, The Minerals, Metals & Materials Society (TMS), Warrendale, PA, 1999.
- 20F. Studsvik laboratory data provided by Anders Jenssen (Studsvik) to MRP Crack Growth Rate Review Team, October 3, 2001 (Proprietary to Studsvik).
- 20G. "Crack Growth Rate Tests of Alloy 600 in Primary PWR Conditions," Communication from M. L. Castaño (CIEMAT) to J. Hickling (EPRI), March 25, 2002.
- 20H. Gómez-Briceño, D., J. Lapeña, and F. Blázquez. "Crack Growth Rates in Vessel Head Penetration Materials," Proceedings of the International Symposium Fontevraud III: Contribution of Materials Investigation to the Resolution of Problems Encountered in Pressurized Water Reactors

- (Chinton, France, September 12-16, 1994), French Nuclear Energy Society, Paris, 1994, pp. 209-214.
- 20I. Gómez-Briceño, D. and J. Lapeña. "Crack Growth Rates in Vessel Head Penetration Materials," Proceedings: 1994 EPRI Workshop on PWSCC of Alloy 600 in PWRs (Tampa, FL, November 15-17, 1994), EPRI, Palo Alto, CA, TR-105406, August 1995, pp. E4-1 through E4-15.
- 20J. Gómez-Briceño, D., et al. "Crack Propagation in Inconel 600 Vessel Head Penetrations", Eurocorr 96, Nice, France, September 24-26, 1996.
- 20K. Castaño, M. L., D. Gómez-Briceño, M. Alvarez-de-Lara, F. Blázquez, M. S. Garcia, F. Hernández, and A. Largares. "Effect of Cationic Resin Intrusions on IGA/SCC of Alloy 600 Under Primary Water Conditions," Proceedings of the International Symposium Fontevraud IV: Contribution of Materials Investigation to the Resolution of Problems Encountered in Pressurized Water Reactors (France, September 14-18, 1998), French Nuclear Energy Society, Paris, 1998, Volume 2, pp. 925-937.
21. "Materials Reliability Program (MRP) Crack Growth Rates for Evaluating Primary Water Stress Corrosion Cracking (PWSCC) of Thick Wall Alloy 600 Material (MRP-55) Revision 1," EPRI, Palo Alto, CA:, November 2002. 1006695.
22. DEI Calculation C-7784-00-4, Rev. 0, "CE Pressurizer Large Heater Sleeve Circumferential Crack Fracture Mechanics Analyses".
23. DEI Calculation C-7784-00-1, Rev. 0, "CE Pressurizer Small Heater Sleeve Stress Analysis".
24. DEI Calculation C-7784-00-2, Rev. 0, "CE Pressurizer Small Heater Sleeve Circumferential Crack Fracture Mechanics Analyses".
25. DEI Calculation C-7784-00-3, Rev. 0, "CE Pressurizer Small Heater Sleeve Circumferential Crack Growth Time to Limiting Flaw Size".
26. NRC Letter, John Stang to Robert P. Powers, Indiana Michigan Power Co., "Issuance of Amendments, D. C. Cook Nuclear Plant, Units 1 and 2", December 23, 1999

## **APPENDIX A: THE EFFECT OF STRESS-STRAIN CURVE CHOICE ON THE ANALYSIS RESULTS**

This stress and fracture evaluation has utilized two sets of stress analyses, which have employed different assumptions as to the stress strain curve. This combination of assumptions resulted from the short time frame in which the analyses needed to be completed, and the fact that one analysis had already been completed when the operability assessment was begun.

The large heater sleeves had already been analyzed when the project began, and had used a monotonic stress strain curve. The small heater sleeve analysis undertaken as part of the project, used a cyclic stress strain curve, to account for the multiple weld passes that are used to weld the heater sleeves, and the strain hardening that accompanies the multiple weld passes.

The cyclic stress-strain curve was determined from laboratory tests carried out on actual reactor vessel head penetration material. The equivalent 0.2% offset yield for this curve is about 50 ksi.

The trend in stresses in a typical head penetration is not affected by the yield stress used in the analysis. Some time ago a series of calculations were carried out to compare the results obtained for a lower stress strain curve, corresponding to a monotonic yield strength of 42.5 ksi, on the exact same geometry, on a reactor vessel head penetration. The results of the comparison for one of the outermost CRDM penetrations is shown in Figures A-1 and A-2.

The trend in stresses, decreasing with distance below the weld, is the same regardless of the yield strength used. In three of the four cases, the actual stress values are higher for the cyclic stress-strain curve. Similar results would be obtained for the heater sleeves, since the geometry is similar.

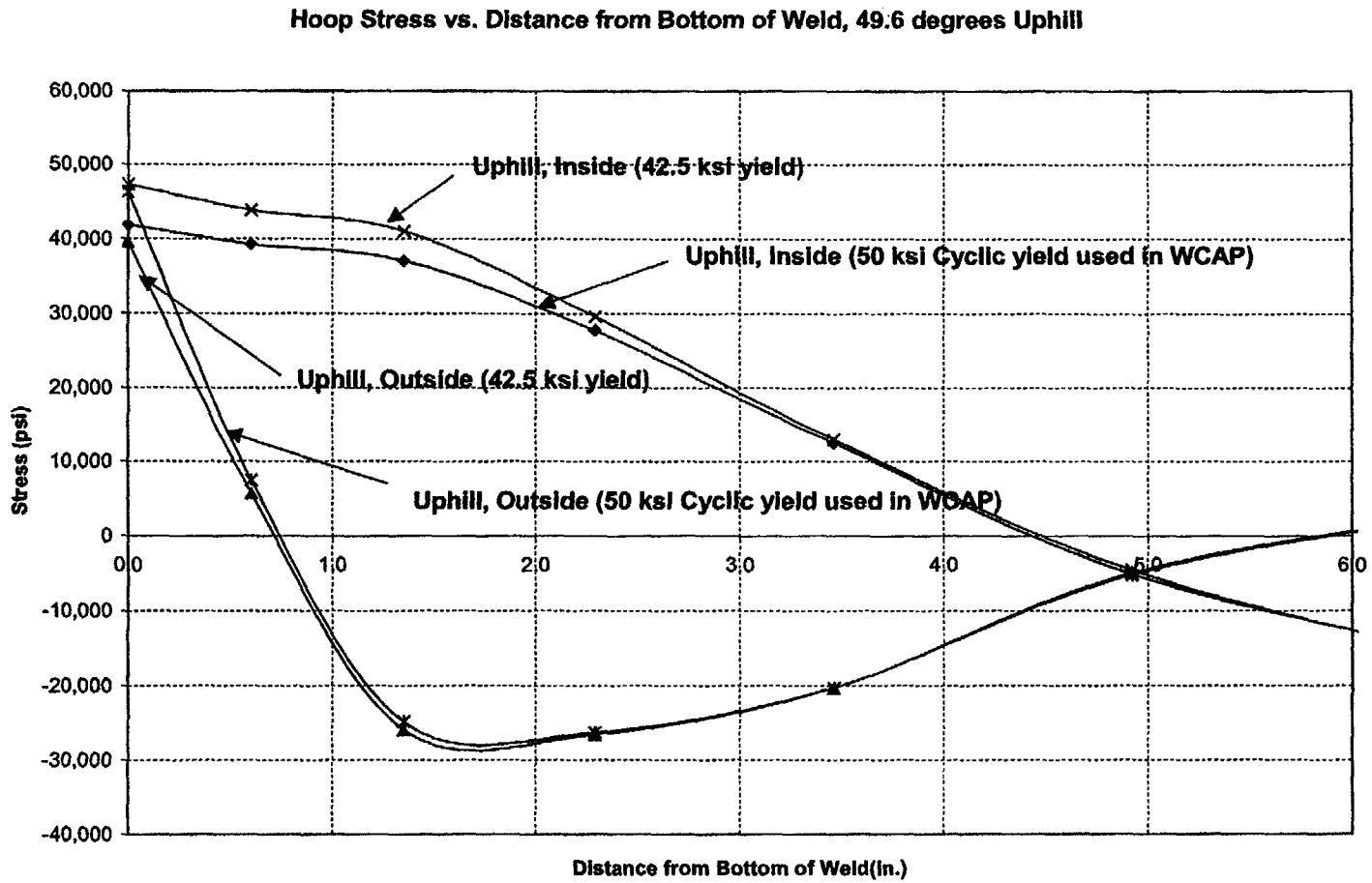


**Figure A-1: Comparison of Monotonic vs Cyclic Stress Strain Curve on Stress Distribution on Uphill Side of a CRDM**

Hoop Stress vs. Distance from Bottom of Weld, 49.6 degrees Downhill

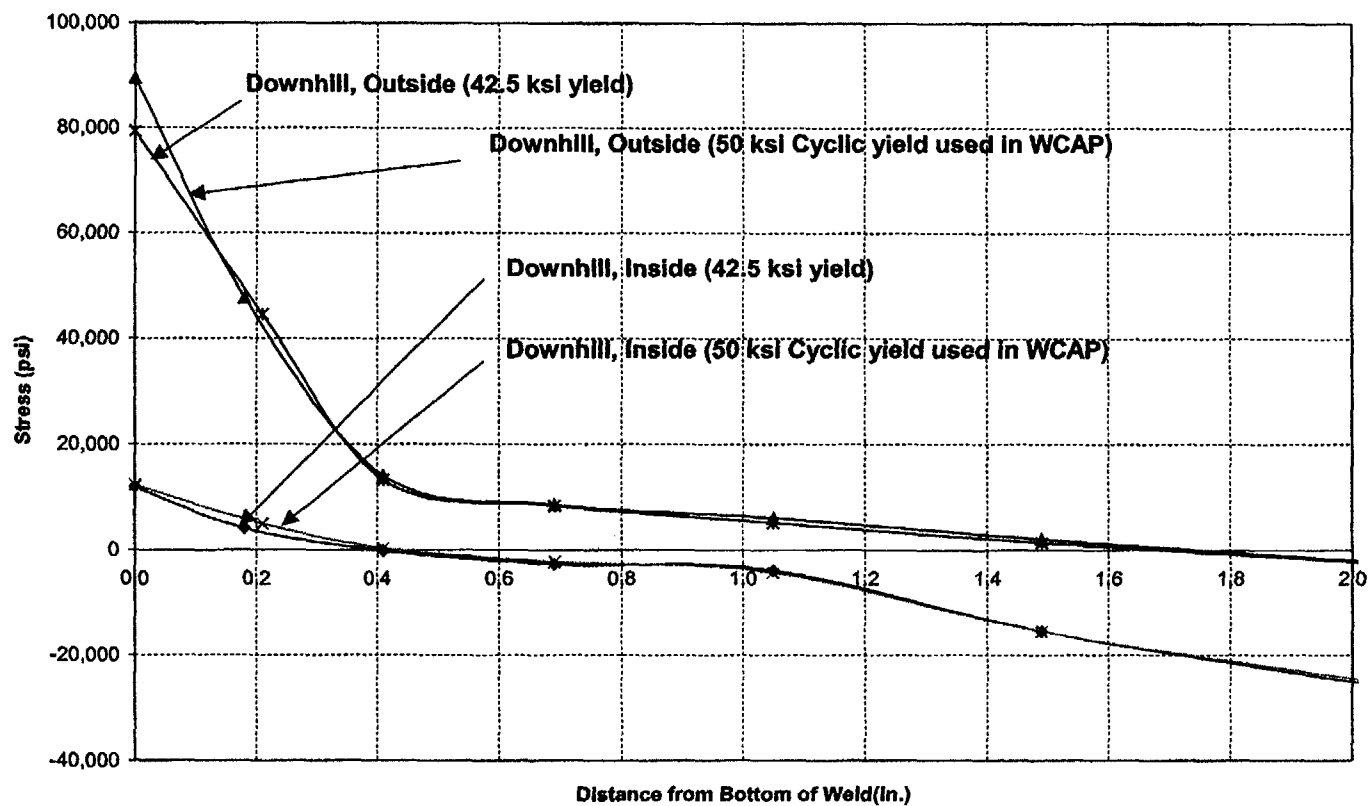


Figure A-2: Comparison of Monotonic vs Cyclic Stress Strain Curve on Stress Distribution on Downhill Side of a CRDM

**WCAP-16180-NP, Rev. 0**



---

**Westinghouse Electric Company, LLC**  
**P.O. Box 355**  
**Pittsburgh, PA 15230-0355**